Magnetic Resonance Temperature Imaging

Baudouin Denis de Senneville, Bruno Quesson, Chrit T. W. Moonen

▶ **To cite this version:**

Baudouin Denis de Senneville, Bruno Quesson, Chrit T. W. Moonen. Magnetic Resonance Temperature Imaging. International Journal of Hyperthermia, 2005, 21 (6), pp.515-531. 10.1080/02656730500133785 . hal-01503868

HAL Id: hal-01503868
https://hal.science/hal-01503868v1

Submitted on 28 Aug 2017

HAL is a multi-disciplinary open access archive for the deposit and dissemination of scientific research documents, whether they are published or not. The documents may come from teaching and research institutions in France or abroad, or from public or private research centers.

L'archive ouverte pluridisciplinaire **HAL**, est destinée au dépôt et à la diffusion de documents scientifiques de niveau recherche, publiés ou non, émanant des établissements d'enseignement et de recherche français ou étrangers, des laboratoires publics ou privés.

Magnetic Resonance Temperature Imaging

B. Denis de Senneville, B. Quesson, C.T.W. Moonen

Invited review

Laboratory for Molecular and Functional Imaging

ERT CNRS, Université « Victor Segalen » Bordeaux 2

Bordeaux, France

Address correspondence to:

C.T.W. Moonen,

Imagerie Moléculaire et Fonctionnelle, ERT CNRS

Université « Victor Segalen » Bordeaux 2

146 rue Leo Saignat, case 117

33076 Bordeaux, France

E-Mail: moonen@imf.u-bordeaux2.fr

Tel: +33 5 57 57 45 86

Fax: +33 5 57 57 45 97

Supported by the "Ligue contre le Cancer", France; the Conseil Regional d'Aquitaine, and Philips Medical Systems.

ABSTRACT

Continuous, real-time 3D temperature mapping during a hyperthermic procedure may provide enhanced safety by visualizing temperature maps in and around the treated region, improved efficiency by adapting local energy deposition with feedback coupling algorithms, and therapy endpoints based on the accumulated thermal dose. Noninvasive mapping of temperature changes can be achieved with MRI, and may be based on temperature dependent MRI parameters. The excellent linearity of the temperature dependency of the proton resonance frequency (PRF) and its near-independence with respect to tissue type make the PRF-based methods the preferred choice for many applications, in particular at mid to high field strength (≥ 0.5 T). The PRF methods employ RF-spoiled gradient echo imaging methods, and incorporate fat suppression techniques for most organs. A standard deviation of less than 1 ^{o}C, for a temporal resolution below 1 s and a spatial resolution of about 2 mm, is feasible for immobile tissues. Special attention is paid to methods for reduction of artifacts in MR temperature mapping caused by intra-scan and inter-scan motion, and motion and temperature-induced susceptibility effects in mobile tissues. Real-time image processing and visualization techniques, together with accelerated MRI acquisition techniques, are described because of their primary importance for real-time, image guided, therapy guidance.

INTRODUCTION

Heat conduction through diffusion and perfusion processes vary locally as a function of tissue architecture, tissue composition, physiological parameters and temperature. Energy deposition at or near the target during thermal therapies depends on the efficiency of absorption of the transmitted energy employing electromagnetic (optical, radiofrequency, microwave) or acoustic waves, and is therefore also a function of tissue composition. Tissue coagulation during the procedure may significantly modify local heat conduction as well as energy absorption. Continuous thermometry appears therefore helpful for assuring adequate thermal treatment in the target region, and avoiding damage to healthy regions. For RF, laser or microwave heating, a needle is inserted in or near the target tissue, and a thermometer is often incorporated in the needle. This allows thermometry at a single point, but does not provide further information on the spatial distribution of temperature for the treatment of a larger volume around the heat source. In case of FUS, the transducer is far from the focal point, generally even outside the body. An inserted thermometer interferes with the ultrasound waves with the wavelengths that are typically used for FUS hyperthermia. Therefore, classical thermometry sensors offer limited value for thermotherapy.

Of the different imaging modalities, MRI appears the ideal tool for temperature mapping. A particular advantage of MRI for guiding thermal procedures is that MRI not only allows temperature mapping but it can be used as well for target definition, and may provide an early evaluation of the therapeutic efficacy. Whereas temperature effects on MR measured parameters (resonance frequency, relaxation, diffusion) had been well described previously, the first report of temperature mapping by MRI appeared in 1983(1). The method was based on the longitudinal relaxation time (T_1). Since then, alternative MR temperature imaging methods have been proposed, based on diffusion coefficient (D) (2), proton resonance frequency (PRF) (3) of tissue water and other temperature-dependent parameters. In this paper, the different methods for MR temperature mapping are reviewed. Special attention is

paid to sensitivity, and linearity of the effects with temperature, their dependence on coagulation, dependence on field strength, and the question whether absolute or relative temperature is measured. In addition, pulse sequences, speed, potential artifacts, and motion sensitivity are discussed for each method, in particular with respect to thermotherapy procedures. Recently, progress in temperature mapping has been reported using ultrasound imaging (4) but these alternative methods still require significant refinement before they can be used for guidance of hyperthermic therapies.

1. Physical basis of temperature MRI methods

1.1 Temperature MRI based on the water proton resonance frequency

The temperature dependence of the water proton resonance frequency (PRF) was first investigated by Hindman for the study of intermolecular forces and hydrogen-bond formation between water molecules (5). MR temperature mapping on the basis of the PRF was first proposed by Ishihara et al. (6) and further developed by de Poorter (7, 8). It is currently the most widely used MR temperature mapping method at mid and high field (0.5T and above). The theory is briefly explained below.

The local magnetic field B_{nuc} as observed by the spins is a function of the main magnetic field B_0 and the temperature T dependent chemical shift field σ:

$$B_{nuc}(T) = (1 + \sigma(T))B_0 \qquad [1]$$

The chemical shift field (in ppm) is the sum of temperature independent contributions, for example those originating from B_0 field inhomogeneities, represented by σ_0, and a temperature dependent contribution, $\sigma_T(T)$:

$$\sigma(T) = \sigma_0 + \sigma_T(T). \qquad [2]$$

The chemical shift field can be calculated from the phase information in RF-spoiled gradient echo images:

$$\Phi(T) = \gamma\sigma(T)T_E B_0 \quad [3]$$

where ϕ is the image phase, γ is the gyromagnetic ratio of the observed nucleus (42.58 10^6 Hz T^{-1} for protons), and TE is the echo time. In order to measure temperature dependent changes in chemical shift, the term σ_0 must be eliminated, which is typically accomplished by subtraction of the field distribution measured at a given reference temperature from the field distribution measured at temperature T, leading to:

$$\Delta T = T - T_{ref} = \frac{\Phi(T) - \Phi(T_{ref})}{\alpha\gamma T_E B_0} \quad [4]$$

where α is the temperature dependency of the water chemical shift in ppm·°C^{-1}.

In principle, any gradient echo method can be used for PRF-based MR thermometry, so long as contributions from stimulated echoes can be neglected (9, 10). RF spoiling of fast gradient echoes is thus necessary when flip angles close to the Ernst angle are used for optimal SNR for short TR. Spin-echo sequences cannot be used since the temperature induced phase contribution will be refocused.

The phase difference between reference data and data acquired during heating increases linearly with the echo time of the experiment, whereas the image signal-to-noise ratio decreases exponentially as a function of TE. Therefore the optimal echo time of the thermometry sequence is equal to the T_2*-value (11, 12). Resulting SNR can be expressed as:

$$SNR = cT_E e^{-\frac{T_E}{T_2^*}} \quad [5]$$

where *c* is a constant, depending on spin density, flip angle, TR, as well as instrumental parameters (field strength, RF coil).

The temperature dependence of the water proton resonance frequency is approximately 0.01 ppm·°C^{-1}. A very important advantage of the PRF method is its near-independence of tissue composition (13). The small remaining tissue dependency may be

related to ion concentration (14). The proportionality constant of PRF with temperature appears at first sight rather low. Comparisons between T_1, D, and PRF based methods have resulted in higher precision for PRF methods (15). An example of PRF-based temperature imaging *in vivo* is shown in Figure 1 (from (16)).

It has been assumed in PRF methods that the macroscopic magnetic susceptibility is independent of temperature, as shown in Equation [2]. However, it has been demonstrated that temperature dependent changes in magnetic susceptibility are not negligible (7, 17, 18). It has been suggested that such effects can be corrected in real-time (19). The presence of lipids is a potential source of artifacts since the PRFs of lipid hydrogens is independent of temperature. Lipids can be conveniently suppressed in gradient echo imaging by frequency-selective slice excitation (10) or alternative methods. PRF-based methods are also sensitive to microscopic susceptibility effects, e.g. related to changes in the concentration of deoxyhemoglobin during the therapy, similar to the BOLD effect (20). Also, strong temperature gradients within a single voxel will lead to a large phase dispersion and hence signal decrease.

Apart from SNR advantages at high field, the sensitivity of the PRF-method increases linearly with the magnetic field strength. However, the exact relationship between sensitivity of PRF-based thermometry and magnetic field strength is not straightforward since gradient echo images are acquired with long TE. The T_2^*-value of the tissue generally decreases with increasing field strength because of macroscopic and microscopic susceptibility effects. Since T_2* contains T_2 and susceptibility contributions, the relation of T_2* with field strength depends on the relative contributions of inhomogeneity and T_2 to the observed T_2^*. If inhomogeneities are dominating, the T_2^* will decrease approximately linearly with increasing field strength, whereas a T_2^*-value close to the T_2-value of the tissue will hardly depend on field strength (assuming T_2 is rather independent of field strength). Note that macroscopic susceptibility effects can be decreased by improving the spatial resolution. An additional

small magnetic field effect originates from the increase in T_1 relaxation time with increasing field resulting in a lower Ernst-angle and in a decreased image SNR.

Non-invasive PRF-based temperature imaging only accounts for relative temperature changes, by comparing a reference image to images acquired under identical experimental conditions. As a consequence, absolute temperature cannot be evaluated. An alternative approach to calculate absolute temperature is MR spectroscopic imaging to measure water resonance shift. The principles of the method are similar to those of PRF with the difference being the acquisition method. Small frequency drifts of the instrument would induce substantial errors on the PRF calculated temperature values whereas proton spectroscopic imaging could include a reference frequency (e.g. lipids (21), N-acetyl-aspartate in brain (22)) and thus be relatively immune to field drifts.

1.2 MR temperature mapping based on other physical mechanisms

1.2.1 Temperature MRI based on the T_1 relaxation time of water protons

The variation in T_1 with temperature can be described by the following relationship (see complete references in (23)).

$$T_1 = T_1(\infty)e^{-\frac{E_a(T_1)}{kT}} \qquad [6]$$

where $E_a(T_1)$ is the activation energy of the relaxation process, k is the Boltzmann constant and T is absolute temperature. Exchange processes between mobile bulk water and relatively immobilized water at surfaces of proteins and membranes play an important role. Within a small temperature range T_1 is linearly dependent on temperature. However, both the T_1 and its temperature dependence differ between tissues. Non-linear effects have been observed in particular when coagulation occurs (24-26). This is not surprising since exchange processes and effective tumbling rates of water may be influenced drastically. Typical changes of T_1

with temperature are of the order of 1%/^{o}C (23). T_1 generally increases from low (<0.5T) to high field (>1T) (27), and T_1 contrast between tissues diminishes. Temperature dependency of T_1 also becomes smaller at higher field strength. Apart from SNR advantages at high field (SNR increases approximately linearly with field strength), temperature mapping based on T_1 is more sensitive at relatively low field strength. T_1 methods generally require more time than PRF based methods. A qualitative overview of the specifications of temperature MRI based on T_1 is given in REF (23).

1.2.2 Temperature MRI based on the molecular diffusion constant of water

The thermal Brownian motion of an ensemble of molecules is characterized by the diffusion constant D. The relationship between temperature and the diffusion constant is exponential

$$D \approx e^{-\frac{E_a(D)}{kT}} \qquad [7]$$

where $E_a(D)$ is the activation energy of the molecular diffusion of water, k is the Boltzmann constant and T is absolute temperature. The dependence of D on temperature can be described as

$$\frac{dD}{DdT} = \frac{E_a(D)}{kT^2}. \qquad [8]$$

As compared to T_1, the activation energy for diffusion of water is substantially higher and the temperature dependency of changes in D amounts to about 2%/°C. Diffusion constants can be measured by MR on the basis of the signal attenuation observed in the presence of a pair of strong mutually counteracting gradients (28).

Despite the good sensitivity of the D method (23), practical problems limit the routine use of the method in vivo. The mobility of water in tissues depends on barriers such as cellular structures, proteins and membranes. This has two major consequences for temperature MRI based on D. Firstly, the dependence of diffusion on temperature is non-

linear since the permeability of such barriers is temperature dependent. Coagulation processes lead to large changes in diffusion constant since diffusion pathways are modified. Non-lethal physiological effects can also lead to large changes in D, for example those observed immediately following ischemia in the brain (D is lowered about 40%) when such changes are still reversible (29). The latter effect has been attributed in part to cell swelling. Similar shifts of water between extracellular spaces and intracellular compartments may also influence D during hyperthermia procedures. Secondly, the mobility of water in tissue is direction-dependent because of the anisotropic nature of the barriers, e.g. in muscle fibers, necessitating full characterization of the diffusion tensor.

It should be noted that diffusion-based temperature MRI methods are based on diffusional displacements of about 10 micrometers via the use of very strong gradient pulses. The methods are therefore also sensitive to macroscopic motion. Apart from SNR advantages at high field and small effects of relaxation times on speed of the imaging methods, temperature mapping based on D is independent of field strength.

1.2.3 Temperature MRI based on changes in bulk magnetization and magnetization transfer rates

The use of some alternative thermometry methods have been suggested, e.g. spin density or magnetization transfer (see (23), and references therein). MR signal strength depends linearly on the magnetization M_0. Since M_0 depends on the Boltzmann thermal equilibrium, it is possible to evaluate temperature changes based on M_0 measurements. However, the temperature dependency is rather small. In addition, when using fast MRI, modifications in M_0 are difficult to separate from effects due to changes in relaxation times. Magnetization transfer depends on chemical exchange of bulk water and labile chemical groups at the surface of proteins and membranes. Such exchange process is temperature-dependent and may be used for MR thermometry. However, the sensitivity of these methods

appears limited and strongly tissue-dependent, and no full analysis is therefore presented in this paper.

1.2.4 Temperature MRI based on temperature-sensitive contrast agents

The temperature sensitivity of some compounds is much higher than that of water. A recent report noted a temperature dependence of more than 1 ppm/^{o}C (30). If such agents can be introduced without toxic side effects at high concentration, the accuracy of proton spectroscopic imaging could be improved. MR spectroscopic imaging is thus a unique tool to non-invasively measure the absolute temperature in vivo, but the low temporal resolution limit its applicability for real-time control of temperature except in case of long treatment duration.

Recently, reports have appeared about novel contrast agents with high temperature sensitivity. Two different mechanisms have been used to render the contrast temperature-sensitive. The first approach was to incorporate conventional contrast agents in temperature-sensitive liposomes (31). Such liposomes do not allow water to exchange between the liposome interior and bulk fluid. Above the transition temperature T_c of the liposome, the membranes become “leaky” for water molecules, and the bulk fluid “feels” the relaxation effect of the contrast agent. The temperature sensitivity is therefore achieved via the exchange process. The second approach is based on a direct, temperature-driven transition between a diamagnetic state to a paramagnetic state using bi-stable molecular complexes (32). A qualitative summary of the principles and performance of the suggested methods is given in REF (23).

2 Advanced temperature MRI

2.1 Rapid MR temperature imaging techniques

Optimal MR thermometry requires high temporal and spatial resolutions to precisely monitor temperature distribution within the targeted organ and to predict the effectiveness of thermal treatment. Ideally, temperature changes are monitored in real-time. In this paper, real-time is defined such that the update time is small compared to a significant temperature change or a temperature change that is potentially hazardous and thus allowing intervention. For example, if the maximum temperature increase is less than 1°C per second, a "real-time" temperature mapping frequency of about 0.1 Hz is sufficient. If the deposited energy might lead to temperature changes of 10°C per second, a much higher temperature mapping frequency is required.

Temperature imaging of the abdomen and thorax is complicated due to complex organ displacement and deformation (mostly resulting from respiration and cardiac cycles), and the presence of flow in large vessels. In addition, magnetic susceptibility is usually spatially inhomogeneous (in particular near intestines, stomach, oesophagi, lungs,…), which may induce important image distortions, especially in the case of rapid phase-sensitive, PRF-based, MR thermometry. A number of rapid imaging sequences, associated with specific reconstruction algorithms, have been developed for near real-time cardiac imaging and functional brain MRI (fMRI). These techniques for scan time reduction were based on the rapid acquisition of the full or a part of k-space (EPI imaging and associated segmented-EPI techniques), or SSFP (True FISP) imaging made possible with the hardware performance of modern scanners. More recently, the use of parallel imaging (eg SENSE (33)) with multiple coils, UNFOLD (34) have opened new possibilities to accelerate image acquisition. These new acquisition methods are very promising for the field or MR thermometry and they could be employed to partially overcome some difficulties of fast PRF thermometry, but with the cost of signal to noise reduction in most of the cases. As a consequence, an optimal compromise has to be made in the choice of the acquisition parameters for a given fast

imaging sequence and a target organ, to avoid a dramatic increase of the uncertainty of phase estimate.

PRF-based temperature MRI methods are based on gradient echoes with long TE (TE approximately equal to T2*). In conventional gradient-echo imaging sequences, the repetition time of the experiment is longer than the echo time. Therefore, a long TE for optimal sensitivity would require also a long TR, and temporal resolution is suboptimal. However, the use of echo shifting (leading to TE>TR in fast gradient echo sequences (35)) avoids this compromise for MRI thermometry (10, 12). So long as the length of the echo train is short compared with TE, a segmented EPI method can be used with multiple read-out periods per TR. When combined with echo-shifting (and maintaining RF spoiling) such a sequence is called a PRESTO sequence (PRinciples of Echo Shifting with a Train of Observation periods, (36)). Therefore, PRF changes can be measured with very fast echo-shifted RF spoiled gradient echoes. Such methods show increased motion sensitivity, and may therefore be useful in immobile tissues.

MRI sequences may be based on radial acquisition of the k-space instead of a standard rectilinear sampling, and thus offer the advantage of being less sensitive to motion. The principle is to acquire central points of k-space at each repetition time and to use these data as navigator echoes to correct each profile displacement.

At present time, a number of studies based on the PRF technique, mainly performed at mid to high field (0.5T-1.5T) have demonstrated that precise temperature imaging can be obtained (37, 38). An example at the lower end of this range is shown in Figure 2.

The use of parallel imaging was successfully tested on human liver at 1.5T(37), as illustrated in Figure 3. Despite signal intensity loss inherent to parallel imaging, scan time reduction of a factor up to 2 could be achieved with a four-element coil, thus reducing artefacts linked to organ displacement. This acceleration of acquisition time can also be used to acquire a larger number of slices over the region of interest. In addition, such parallel

imaging techniques could be very useful at high fields (typically 3T), taking advantage of the increase of signal intensity. In combination with segmented EPI acquisition techniques, parallel imaging can also be used to reduce the echo train length per repetition time at constant imaging time, with the advantage of reducing image distortions due to susceptibility effects.

The use of balanced fast field echoes sequences (SSFP, Balanced FFE, TrueFISP) was also investigated to derive temperature maps(39, 40). The advantage of this fast imaging technique is to offer high image quality with excellent anatomical detail. However, the PRF effect of the MR signal in such sequences is non-linear, and hard to separate from dynamic susceptibility effects. Its value for in vivo temperature mapping needs to be evaluated.

Despite MR thermometry was successfully tested on several organs at low (0.2T), mid (0.5T) and high field (≥1.5T), it remains necessary to improve volumetric coverage of the region of interest in mobile tissues, to precisely characterize local distribution of the temperature in the pathologic target and in surrounding healthy tissue. Novel techniques like slice tracking and real-time adaptive image techniques may become useful additions to the modern, PRF based, fast temperature imaging methods. Also, it is expected that the PRF methods will show improved performance at high field

3 Real-time image processing

As PRF-based temperature maps result from phase differences, this technique is prone to motion artefacts (patient motion, respiration, cardiac activity) (41). When physical causes of the artifacts are reduced with the use of rapid imaging and image monitoring methods (see also section 3.3), image processing techniques can be used to further improve the quality of the thermometry. Processing of an image must be done fast to ensure real-time monitoring of temperature evolution (see also section 2.2). In practical terms, this implies that image processing must be done well within the update time between subsequent images.

3.1 Time scale of motion artifacts

Motion artefacts during MR thermometry sequence can be divided in two categories, intra-scan and inter-scan motion, based on the time scale of the motion as compared to the image acquisition time.

a) Intra-scan motion

This artifact is caused by the movement of an object during MR signal readout, yielding a low quality image, showing typical ghosting and blurring in the phase-encode direction. This artifact can be reduced by accelerating the imaging technique. However, a compromise on the acquisition parameters has to be made to obtain sufficient SNR while shortening acquisition duration. In the case of respiratory motion, typical acquisition duration of 400ms for one slice was found to be a reasonable value to obtain a sufficient SNR and to avoid intra-scan motion artifacts. On-line correction of this artifact is routinely performed during the image reconstruction process on state-of-the-art MRI instruments.

b) Inter-scan motion

Good image quality is obtained with moving organs but the region of interest is not correctly registered between successive images. This artifact can be generated by reflex or accidental patient motion and periodic motion like respiratory or cardiac activity.

Thermometry artifacts generated by motion of the susceptibility field

Although the spatial transformation of the reference phase image can be corrected, an unwanted phase shift cannot be fully suppressed. In fact, the local magnetic susceptibility is generally not fully uniform and the resulting phase variation $\Delta\varphi$ can be described by the following equation (19) :

$$\Delta\varphi = \gamma.\alpha.B_0.\Delta T.T_E + \gamma.B_0.FT^{-1}\left[\left(\frac{1}{3} - \frac{K_Z^2}{K^2}\right).FT(\Delta\chi)\right].T_E, \quad K \neq 0 \qquad [9]$$

where $K = (K_X, K_Y, K_Z)$ the position vector in the reciprocal space, and $\Delta\chi$ the modification of the susceptibility field. The other terms have been described above. The first term of the sum is due to the PRF-shift with temperature, whereas the second term arises when an object motion occurs. Both PRF-shift with temperature and movement of the patient lead to phase variation and it is not possible to separate the two contributions within a single phase image. Modeling of inhomogeneous field of susceptibility in-vivo is difficult and the sensitivity of PRF thermometry has limited its application to immobile organs and organs that can be easily restrained like muscle (42), breast (43) and the prostate (14).

However, strategies allow correcting inter-scan motion related errors in PRF based MR thermometry, avoiding explicit modeling of the susceptibility field. Those techniques require first to estimate motion.

3.2 Motion reduction techniques

Motion restraining devices in the positioning of the patient are helpful. In addition, motion artefacts can be reduced significantly using rapid imaging techniques and navigator echoes. The simplest technique to reduce periodic motion artifacts is to synchronize the acquisition of the images to a stable period of the cycle (e.g. at the end of expiration for breathing). On line evolution of the respiration can be monitored with external methods using a pressure sensor positioned on the abdomen of the subject. Synchronization can be achieved by triggering the MR pulse sequence based on signals provided by the sensor ("respiratory gating" (44). Alternatively MR methods can be employed using so-called navigator echoes (45)). The major drawback of those methods is that the temporal resolution depends on the motion frequency and a limited set of images can be acquired during a respiratory cycle (~ 5 seconds for humans).

3.3 Physical methods for estimation of motion

Navigator echoes

Navigator echoes use an approach that consists of acquiring one or multiple lines of Fourier space including the center and applying an inverse Fourier transformation in order to obtain the profile of the object. This profile can be use to estimate motion (45). However, the use of navigator echoes is restricted to rigid body motion and may not be optimal for complex organs displacements and/or deformations such as in the abdomen (liver, kidney) and the heart.

Ultrasonic echo

By sending an ultrasonic wave to a reflective target and measuring the time of flight for the return of this signal, the distance between the source and the target can be computed by multiplying this time by the speed of sound. This technique allows estimating the 3D translation of a point located in an unheated region. In general, the displacement of the heated region is hard to estimate in vivo because the coagulation caused by the heating modifies the echo. The technique is based on the hypothesis that the whole studied region undergoes the same displacement. Only the displacement of a point source of the target is obtained. This technique has been successfully used to target a mobile organ with an external heating source (for example with a focus ultrasound device) (46).

Active tracking coil

An active tracking coil can be used to obtain the 3D coordinates relative to the heat source location (47). The active tracking coil is integrated into a power laser sheath that is introduced into the object. A custom receiver is used to detect location information from the active coil. Like the preceding approach, only the displacement of a point source of the target is obtained.

3.4 Estimation of motion based on image registration techniques

This approach consists of using image processing techniques to detect organs displacements on the anatomic images. The objective is to relate the coordinate of each part of tissue in the image to register with the corresponding tissue in the reference image. Contrary to the methods described above, complex organs displacements can be successfully estimated. To allow on-line monitoring of MR thermometry, this approach requires the use of a registration method that estimates motion on images under the following conditions

- no specification of the observed organ
- no user intervention
- real-time implementation.

In practice, under on-line conditions, it is often not practical to acquire isotropic 3D temperature maps on mobile organs, due to technical limitations of MR hardware and acquisition sequences. Thus, it is difficult to perform 3D image registration and one practical approach consists of estimating organ displacements in a 2D image generated from objects that are moving in 3D space (41). Slices must be oriented in the principal axis of the organ displacement so that apparent movement is the best approximation of the real movement. Image based registration can be divided in the following approaches :

Methods based on artificial foreign objects attached to the patient

Generally, such registration methods *(48)* are difficult to be used for non-invasive MR therapy because :

- invasive markers cannot obviously be used (49, 50).
- the nature of the registration transformation is often restricted to be rigid (51-53).

Methods based on patient generated image information only

Motion can be estimated on a set of landmarks, segmented structures, or computed directly from the image intensities *(54)*:

-Methods based on landmarks may not be practical in our case because user interaction is required for the identification of the landmarks (55) and the real-time control necessitates robust, and preferably automatic, methods.

-Segmentation based methods (with region extraction like deformable models (56), geometrical characteristic computation like high curvature pixels (57), or zeroing of the Laplacian (58), etcetera) could be used but, in practice, the segmentation techniques depend on the observed organ and the computation time is often not compatible with the real-time constraint. Moreover, the registration accuracy depends on the accuracy of the segmentation step.

-Methods based on image intensities without user prioritization or segmentation step. Since some implementations of these algorithms are fast, and they do not require specifications with respect to the organ of interest nor any other user interaction, this approach is compatible with the conditions required to allow on-line monitoring of MR thermometry.

Two approaches may be followed:

-Global transformation estimation using: a) principal axes and moments based methods (rigid motions are estimated with the spatial distribution of their mass (59)); b) Fourier-based image registration algorithm (the properties of invariance in rotation and translation are used (60)); this method can register 2D images that are misaligned due to translation, rotation and scale (61)); c) based on a parameterized model of motion (62) (identification of the displacement is done by optimizing model parameters).

-Local transformation estimation using: a) block-Matching (the image to be registered is divided in blocks and the translation of each block is estimated in a research window (63); it is supposed that the motion in the image is constant in the block; b) differential estimation

methods of the optical flow (a velocity field is estimated assuming that intensity is conserved during displacement). A regularity constraint is also required, like 1) local regularity constraint that may optimize some local energy expression (64) or 2) global regularity constraint which attempts to minimize a global energy function(65)). This kind of method may be very useful for organs with complex motion and distortion like liver and heart.

3.5 Motion correction for on-line MR thermometry

Referenceless PRF Shift thermometry

This approach estimates the background phase from each acquired image phase. A polynomial fit to the background phase outside the heated region is performed using a weighted least-squares fit. Extrapolation of the polynomial to the heated region serves as the background phase estimate, which is then subtracted from the actual phase (66).

The major drawbacks of this approach are :

-The phase in the heated region is deduced from the phase outside the heated region. It is possible only if the susceptibility in the object is uniform. In addition, the phase ϕ has to be unwrapped. Phase discontinuities may be problematic.

-The method requires that phase perturbation induced by motion and by frequency drift during the intervention can be precisely expressed with a mathematical function (it depends on susceptibility in the observed organs and its neighbours but also of the actual motion).

-The method requires that enough pixels with sufficient SNR are located outside the heated region in order to allow a robust approximation of the mathematical function. In MR thermometry sequence, lipid suppression often generates images without sufficient signal in some locations. In addition, this method may be difficult to use when heated regions are close to interfaces between organs with different magnetic susceptibilities (lung/liver) or signal content (fat/water).

Correct spatial reference for thermometry

If a motion occurs between the instant t_{n-1} and t_n, the relative temperature map after motion may be erroneous. A simple method consists of detecting motion vector to correct phase and temperature maps (67). Then the phase image acquired at t_n (φ_n) is taken as new phase image reference, and the temperature mapping at t_i ($i > n$) is computed with :

$$\Delta T_i = \Delta T' + (\varphi_i - \varphi_n).k \quad [16]$$

where $\Delta T'$ is the n-1 temperature map after motion correction. Using this method, information about temperature changes between the instant t_{n-1} and t_n is lost. Moreover, as mentioned previously (45), noise in the temperature map increases with the number of images corrupted by motion in a time series. In addition, uncertainty induced by the correction technique is propagated through all images obtained after each displacement. As a consequence, this technique can be applied when periodic motion has already been corrected with synchronization techniques.

Multi-baseline

A collection of multiple baseline reference images can be used to generate temperature maps. The selection of baseline image for temperature computation can be based on navigator echoes data, on the displacement of an active tracking coil (47), or on the displacement estimate on anatomical images with image registration algorithms (68). This approach can be used either to perform rapid acquisition (acquisition time per image faster than typical motion period) without synchronisation techniques in order to improve the temporal resolution (47, 68), or to improve the quality of the thermometry when periodical motion is reduced (69).

3.6 Image quality test

It is necessary to use a quality criterion to test the image processing efficiency. Indeed, intra-scan motion and modification of the image plane position by through-plane motion can be detected rapidly. It is thus possible to detect those motion-corrupted images by using a real-time evaluation of a similarity criterion between the acquired anatomical images and a reference image (37, 47). Images that do not match the quality criterion should not be included in the thermometry process.

Conclusion

The excellent linearity of the temperature sensitivity of the water PRF and its near-independence with respect to tissue type, together with good temperature sensitivity, make PRF based temperature MRI the preferred choice for many applications, in particular at mid or high field ($\geq$ 1 T), and probably even at very high field ($\geq$ 3T). The PRF methods employ RF-spoiled gradient echo imaging methods in order to measure the phase change resulting from temperature-dependent changes in resonance frequency. When combined with modern parallel imaging techniques and other acceleration methods, the PRF based temperature maps can be acquired rapidly. A standard deviation of less than 1 ^{o}C for a temporal resolution below 1 s and a spatial resolution of about 2 mm is feasible for a single slice for immobile tissues. The rapid PRF methods generally allow only relative temperature measurements and fat suppression is necessary for most tissues. The methods require excellent registration to correct for displacements between scans since temperature maps are derived from relative changes between images. Navigator echoes and advanced image processing tools can be employed to detect and correct intra and inter-scan motion artifacts in real-time. Such tools will become indispensable for accurate guidance and control of local thermal therapies, in particular when treating mobile tissues.

REFERENCES

1. Parker DL, Smith V, Sheldon P, Crooks LE, Fussell L. Temperature distribution measurements in two-dimensional NMR imaging. Med Phys 1983;10(3):321-5.

2. Le Bihan D, Delannoy J, Levin RL. Temperature mapping with MR imaging of molecular diffusion: application to hyperthermia. Radiology 1989;171(3):853-7.

3. Ishihara Y, Calderon A, Watanabe H, Okamoto K, Suzuki Y, Kuroda K, et al. A precise and fast temperature mapping using water proton chemical shift. Magn Reson Med 1995;34(6):814-23.

4. Pernot M, Tanter M, Bercoff J, Waters KR, Fink M. Temperature estimation using ultrasonic spatial compound imaging. IEEE Trans Ultrason Ferroelectr Freq Control 2004;51(5):606-15.

5. Hindman J. Proton resonance shift of water in the gas and liquid states. J Chem Phys 1966;44:4582-4592.

6. Ishihara Y, Calderon A, Watanabe H, Mori K, Okamoto K, Suzuki Y, et al. A precise and fast temperature mapping method using water proton chemical shift. Proc SMRM, Berlin 1992:4803.

7. De Poorter J. Noninvasive MRI thermometry with the proton resonance frequency method: study of susceptibility effects. Magn Reson Med 1995;34(3):359-67.

8. De Poorter J, De Wagter C, De Deene Y, Thomsen C, Stahlberg F, Achten E. Noninvasive MRI thermometry with the proton resonance frequency (PRF) method: in vivo results in human muscle. Magn Reson Med 1995;33(1):74-81.

9. Chung YC, Duerk JL. Signal formation in echo-shifted sequences. Magn Reson Med 1999;42(5):864-75.

10. de Zwart JA, Vimeux FC, Delalande C, Canioni P, Moonen CT. Fast lipid-suppressed MR temperature mapping with echo-shifted gradient- echo imaging and spectral-spatial excitation. Magn Reson Med 1999;42(1):53-9.

11. Chung AH, Hynynen K, Colucci V, Oshio K, Cline HE, Jolesz FA. Optimization of spoiled gradient-echo phase imaging for in vivo localization of a focused ultrasound beam. Magn Reson Med 1996;36(5):745-52.

12. de Zwart JA, van Gelderen P, Kelly DJ, Moonen CT. Fast magnetic-resonance temperature imaging. J Magn Reson B 1996;112(1):86-90.

13. Peters RD, Hinks RS, Henkelman RM. Ex vivo tissue-type independence in proton-resonance frequency shift MR thermometry. Magn Reson Med 1998;40(3):454-9.

14. Peters RD, Chan E, Trachtenberg J, Jothy S, Kapusta L, Kucharczyk W, et al. Magnetic resonance thermometry for predicting thermal damage: an application of interstitial laser coagulation in an in vivo canine prostate model. Magn Reson Med 2000;44(6):873-83.

15. Wlodarczyk W, Boroschewski R, Hentschel M, Wust P, Monich G, Felix R. Three-dimensional monitoring of small temperature changes for therapeutic hyperthermia using MR. J Magn Reson Imaging 1998;8(1):165-74.

16. McDannold N, King RL, Hynynen K. MRI monitoring of heating produced by ultrasound absorption in the skull: in vivo study in pigs. Magn Reson Med 2004;51(5):1061-5.

17. Peters RD, Hinks RS, Henkelman RM. Heat-source orientation and geometry dependence in proton-resonance frequency shift magnetic resonance thermometry. Magn Reson Med 1999;41(5):909-18.

18. Young IR, Hajnal JV, Roberts IG, Ling JX, Hill-Cottingham RJ, Oatridge A, et al. An evaluation of the effects of susceptibility changes on the water chemical shift method of temperature measurement in human peripheral muscle. Magn Reson Med 1996;36(3):366-74.

19. Salomir R, Denis de Senneville B, Moonen CTW. A fast calculation method for magnetic field inhomogeneity due to an arbitrary distribution of bulk susceptibility. Concepts in Magnetic Resonance 2003;Vol. 19B(1):26-34.

20. Ogawa S, Lee TM, Kay AR, Tank DW. Brain magnetic resonance imaging with contrast dependent on blood oxygenation. Proc Natl Acad Sci U S A 1990;87(24):9868-72.

21. Kuroda K, Oshio K, Chung AH, Hynynen K, Jolesz FA. Temperature mapping using the water proton chemical shift: a chemical shift selective phase mapping method. Magn Reson Med 1997;38(5):845-51.

22. Cady EB, D'Souza PC, Penrice J, Lorek A. The estimation of local brain temperature by in vivo 1H magnetic resonance spectroscopy. Magn Reson Med 1995;33(6):862-7.

23. Quesson B, de Zwart JA, Moonen CT. Magnetic resonance temperature imaging for guidance of thermotherapy. J Magn Reson Imaging 2000;12(4):525-33.

24. Fried MP, Morrison PR, Hushek SG, Kernahan GA, Jolesz FA. Dynamic T1-weighted magnetic resonance imaging of interstitial laser photocoagulation in the liver: observations on in vivo temperature sensitivity. Lasers Surg Med 1996;18(4):410-9.

25. Graham SJ, Bronskill MJ, Henkelman RM. Time and temperature dependence of MR parameters during thermal coagulation of ex vivo rabbit muscle. Magn Reson Med 1998;39(2):198-203.

26. Graham SJ, Stanisz GJ, Kecojevic A, Bronskill MJ, Henkelman RM. Analysis of changes in MR properties of tissues after heat treatment. Magn Reson Med 1999;42(6):1061-71.

27. Bottomley PA, Foster TH, Argersinger RE, Pfeifer LM. A review of normal tissue hydrogen NMR relaxation times and relaxation mechanisms from 1-100 MHz: dependence on tissue type, NMR frequency, temperature, species, excision, and age. Med Phys 1984;11(4):425-48.

28. Delannoy J, Chen CN, Turner R, Levin RL, Le Bihan D. Noninvasive temperature imaging using diffusion MRI. Magn Reson Med 1991;19(2):333-9.

29. Moseley M, Cohen Y, Mintorovitch J, Kucharczyk J, Weinstein P. Early detection of cerebral ischemia in cats: comparison of diffusion- and T2-weighted MRI and spectroscopy. Magn Reson Med 1990;14:330.

30. Aime S, Botta M, Fasano M, Terreno E, Kinchesh P, Calabi L, et al. A new ytterbium chelate as contrast agent in chemical shift imaging and temperature sensitive probe for MR spectroscopy. Magn Reson Med 1996;35(5):648-51.

31. Fossheim SL, Il'yasov KA, Hennig J, Bjornerud A. Thermosensitive paramagnetic liposomes for temperature control during MR imaging-guided hyperthermia: in vitro feasibility studies. Acad Radiol 2000;7(12):1107-15.

32. Bartholet A, Goudemant J, Laurent S, Kahn O, Vander Elst L, Muller R. Spin transition Molecular Materials: Intelligent Contrast Agents for Magnetic Resonance Thermometry. ISMRM abstract 2000.

33. Pruessmann KP, Weiger M, Scheidegger MB, Boesiger P. SENSE: sensitivity encoding for fast MRI. Magn Reson Med 1999;42(5):952-62.

34. Madore B, Glover GH, Pelc NJ. Unaliasing by fourier-encoding the overlaps using the temporal dimension (UNFOLD), applied to cardiac imaging and fMRI. Magn Reson Med 1999;42(5):813-28.

35. Moonen CT, Liu G, van Gelderen P, Sobering G. A fast gradient-recalled MRI technique with increased sensitivity to dynamic susceptibility effects. Magn Reson Med 1992;26(1):184-9.

36. Liu G, Sobering G, Duyn J, Moonen C. A functional MRI technique combining principles of Echo-Shifting with a train of observations (PRESTO). Magn. Reson. Med. 1993;30:764-768.

37. Weidensteiner C, Kerioui N, Quesson B, de Senneville BD, Trillaud H, Moonen CT. Stability of real-time MR temperature mapping in healthy and diseased human liver. J Magn Reson Imaging 2004;19(4):438-46.

38. Weidensteiner C, Quesson B, Caire-Gana B, Kerioui N, Rullier A, Trillaud H, et al. Real-time MR temperature mapping of rabbit liver in vivo during thermal ablation. Magn Reson Med 2003;50(2):322-30.

39. Paliwal V, El-Sharkawy AM, Du X, Yang X, Atalar E. SSFP-based MR thermometry. Magn Reson Med 2004;52(4):704-8.

40. Scheffler K. Fast frequency mapping with balanced SSFP: theory and application to proton-resonance frequency shift thermometry. Magn Reson Med 2004;51(6):1205-11.

41. Denis de Senneville B, Desbarats P, Quesson B, Moonen CTW. Real-Time Artefact Corrections For Quantitative MR Temperature Mapping. Journal of WSCG 2003;Vol.11(1).

42. Hazle JD, Stafford RJ, Price RE. Magnetic resonance imaging-guided focused ultrasound thermal therapy in experimental animal models: correlation of ablation volumes with pathology in rabbit muscle and VX2 tumors. J Magn Reson Imaging 2002;15(2):185-94.

43. Hynynen K, Pomeroy O, Smith DN, Huber PE, McDannold NJ, Kettenbach J, et al. MR imaging-guided focused ultrasound surgery of fibroadenomas in the breast: a feasibility study. Radiology 2001;219(1):176-85.

44. Morikawa S, Inubushi T, Kurumi Y, Naka S, Sato K, Demura K, et al. Feasibility of respiratory triggering for MR-guided microwave ablation of liver tumors under general anesthesia. Cardiovasc Intervent Radiol 2004;27(4):370-3.

45. de Zwart JA, Vimeux FC, Palussiere J, Salomir R, Quesson B, Delalande C, et al. On-line correction and visualization of motion during MRI-controlled hyperthermia. Magn Reson Med 2001;45(1):128-37.

46. Pernot M, Tanter M, Fink M. 3D Real-time Motion Correction in High Intensity Focused Ultrasound Therapy. Ultrasound Medicine and Biology 2004.

47. Suprijanto S, Vogel MW, Vos FM, Vrooman HA, Vossepoel AM. Displacement Correction Scheme for MR-Guided Interstitial Laser Therapy. Lecture Notes in Computer Science 2879 2003;2.

48. Lemieux L, Jagoe R. Effects of fiducial marker localization on stereotactic target coordinate calculation in CT slices and radiographs. Physics in medicine and biology 1994;39(11):1915-1928.

49. Maurer C. R. FJM, Galloway R. L., Wang M. Y., Maciunas R. J., Allen G. S. The accuracy of image-guided neurosurgery using implantable fiducial markers. In Lemke H. U., Inamura K., Jaffe C. C., and Vannier M. W. (eds) 1995:1197-1202.

50. Maurer CR, Fitzpatrick JM. A review of medical image registration. Maciunas, R. J. (ed.) 1993:17-44.

51. Maguire GQ, Noz M, Rusinek H, Jaeger J, Kramer EL, Sanger JJ, et al. Graphics applied to medical image registration. 1991;11(2):20-28.

52. Leslie WD, Borys A, McDonald D, Dupont JO, Peterdy AE. External reference markers for the correction of head rotation in brain single-photon emission tomography. Eur J Nucl Med 1995;22(4):351-5.

53. Simon DA, O'Toole RV, Blackwell M, Morgan F, DiGioia AM, Kanade T. Accuracy validation in image-guided orthopaedic surgery. Medical robotics and computer assisted surgery 1995:185-192.

54. Maintz JB, Viergever MA. A survey of medical image registration. Med Image Anal 1998;2(1):1-36.

55. Evans AC, Marett S, Collins L, Peters TM. Anatomical-functional correlative analysis of the human brain using three dimensional imaging systems. In Schneider R. H., Dwyer III S? J., and jost R. G. (eds), Medical imaging: image processing 1989;1092:264-274.

56. Gueziec A. Large deformable splines, crest lines and matching. In International conference on computer vision 1993:650-657.

57. Davis LS, Wu Z, Sun H. Contour-Based Motion Estimation. Graphics and Image Processing 1983;vol. 23, no. 3:313-326.

58. Hildreth EC. The computation of the velocity field. Proc R Soc Lond B Biol Sci 1984;221(1223):189-220.

59. Hu MK. Visual pattern recognition by moment invariants. IEEE Trans. Inform. Theory 1962;5:179-187.

60. De Castro E, Morandi C. Registration of translated and rotated images using finite Fourier transforms. IEEE Trans. Pattern Anal. Mach. Intell. 1987;9(5):700-703.

61. Reddy BS, Chatterji DN. An fft-based technique for translation, rotation, and scale-invariant image registration. IEEE Trans. Pattern Analyses and Machine Intelligence 1996;5(8):1266-1270.

62. Friston KJ, Ashburner J, Frith CD, Poline J-B, Heather JD, Frackowiak RSJ. Spatial registration and normalisation of images. Human Brain Mapping 1995;2:165-189.

63. Chen MJ, Chen LG, Chiueh TD, Lee YP. A New Block-Matching Criterion for Motion Estimation and Its Implementation. IEEE Trans. on Circuits and Systems for Video Technology 1995;5(3):231-236.

64. Lucas BD, Kanade T. An Iterative Image Registration Technique with an Application to Stereo Vision. In: Proceedings of the 7th International Joint Conference on Artificial Intelligence; 1981; Vancouver; 1981. p. 674-679.

65. Schunck BG, Horn BKP. Determining optical flow. Artificial Intelligence 1981;17:185-203.

66. Rieke V, Vigen KK, Sommer G, Daniel BL, Pauly JM, Butts K. Referenceless PRF shift thermometry. Magn Reson Med 2004;51(6):1223-31.

67. Denis de Senneville B, Desbarats P, Salomir R, Quesson B, Moonen CTW. Correction Of Accidental Patient Motion For On-line MR Thermometry. In; 2004 September 26-29; Saint Malo, France: Medical Image Computing and Computer-Assisted Intervention; 2004. p. 637-644.

68. Denis de Senneville B, Quesson B, Desbarats P, Salomir R, Palussière J, Moonen CTW. Atlas-Based Motion Correction For On-Line MR Temperature Mapping. In: IEEE International Conference On Image Processing; 2004; Singapore; 2004.

69. Vigen KK, Daniel BL, Pauly JM, Butts K. Triggered, navigated, multi-baseline method for proton resonance frequency temperature mapping with respiratory motion. Magn Reson Med 2003;50(5):1003-10.

70. Botnar RM, Steiner P, Dubno B, Erhart P, von Schulthess GK, Debatin JF. Temperature quantification using the proton frequency shift technique: In vitro and in vivo validation in an open 0.5 tesla interventional MR scanner during RF ablation. J Magn Reson Imaging 2001;13(3):437-44.

FIGURES

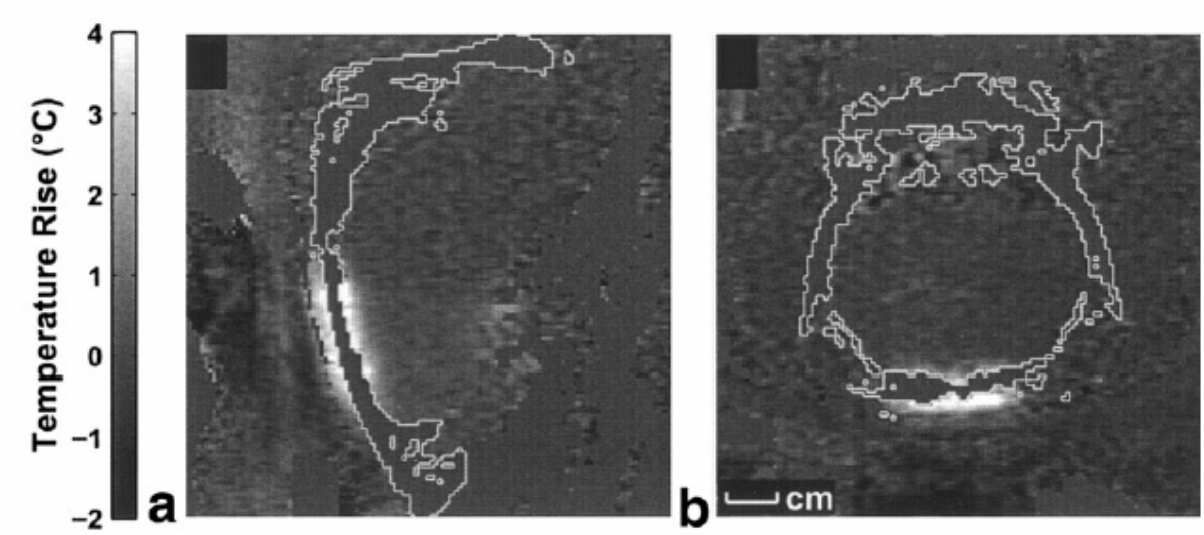

Figure. 1: MR images showing the peak temperature increase after a 10-W sonication. Left: Sagittal scans. Right: Axial scans. The contours indicate the skull (for details see (16)).

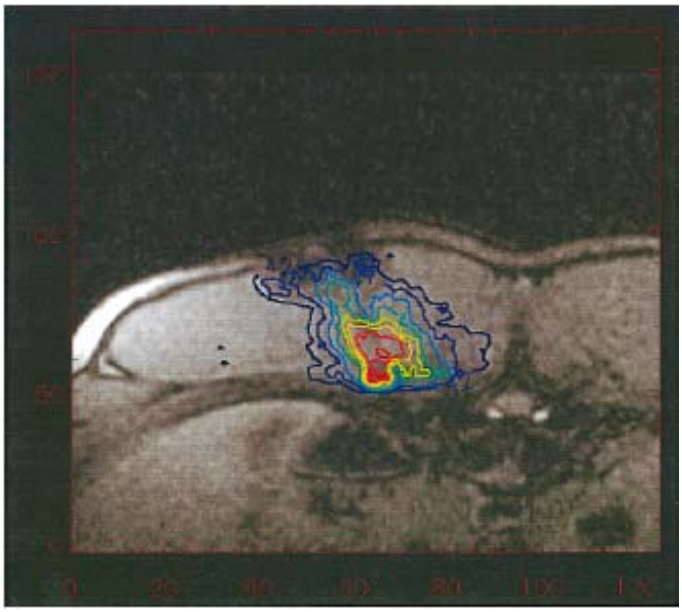

Figure 2. Isotherms following 6 minutes RF energy deposition in the paraspinal muscle of an anesthetized pig. The step size is 5°C. Due to physiologic blood circulation, heat dissipation is more variable than it is in the ex vivo muscle (for complete details see (70)).

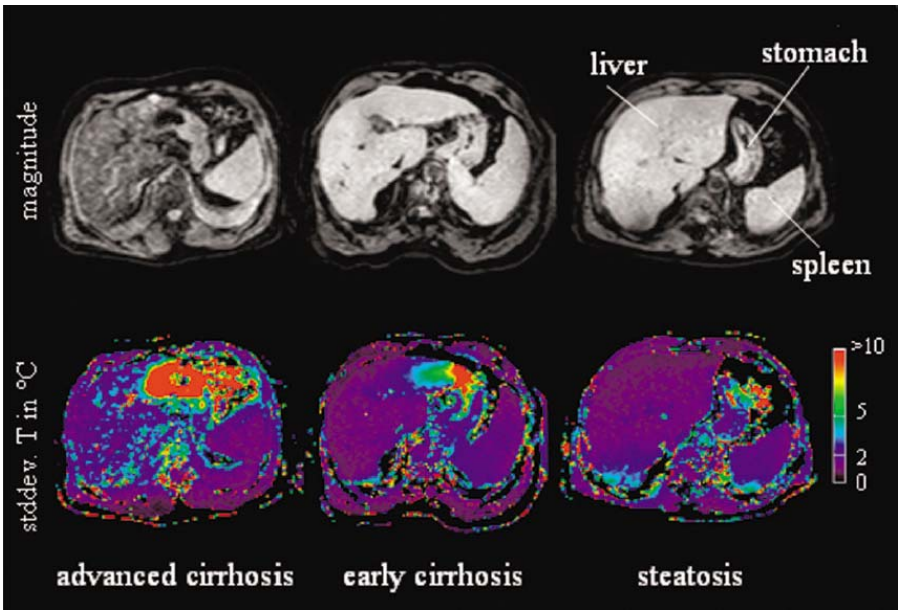

Figure 3 : Transversal images in three liver tumor patients acquired with the respiratory-gated SENSE-EPI sequence, together with corresponding color-coded maps of the temperature SD of a time series of temperature maps. The precision of temperature maps was calculated from phase stability maps at body temperature (for further details see (37)).

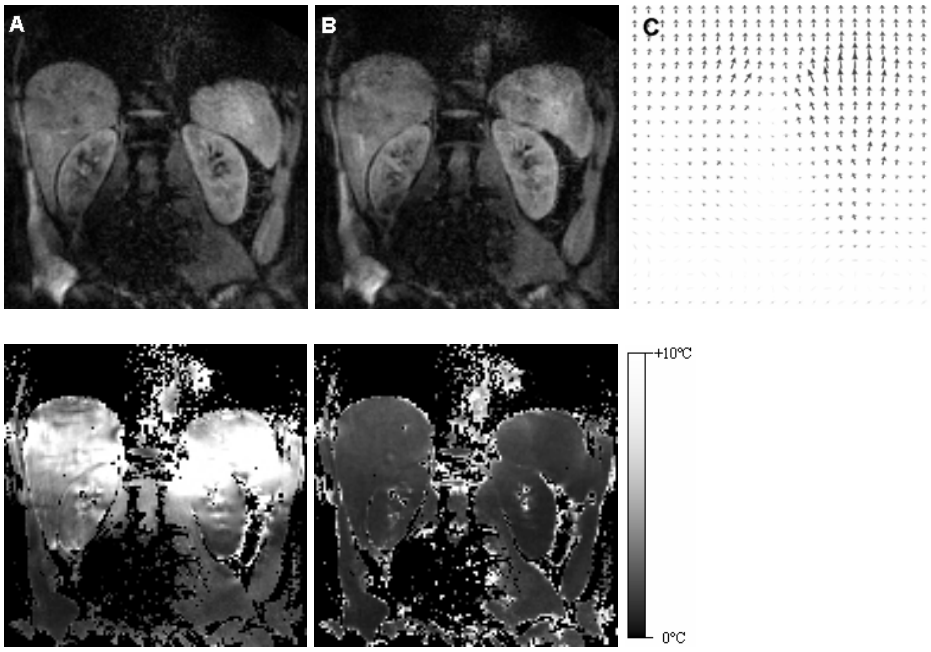

Figure 4 : example of motion correction in temperature mapping of the abdomen a a healthy free breathing volunteer. (A) & (B) show MR anatomical images obtained at different times. (C) represents the Motion field estimation. Temporal standard deviation (see right for the scale) of the temperature on each pixel of the abdomen before (D) and after (E) correction. (For complete details, see (68)).